Introduction

Elastic full waveform inversion (EFWI) is formulated as a nonlinear inverse problem constrained by an elastic wave equation and it works by iteratively minimizing an objective function that computes the misfit between observed and modelled data in the least-squares sense. Compared to the acoustic formulation, EFWI better describes the subsurface properties (Tarantola, 1988; Pratt, 1990; Plessix, 2006), as it takes into account elastic phenomena and thus adequately describes significant wave propagation mechanisms, such as mode conversions and the correct amplitude behavior of seismic waves. However, EFWI is hampered by significant problems (Operto et al., 2013). First, the objective function is multimodal and depending on the numerical optimization technique, the solution of the inverse problem may represent a local minimum. This phenomenon is due to cycle skipping which occurs when the starting models are unable to predict data that match the observed data to better than half a cycle at the lowest usable frequencies available in the data set. Second, inversion implementations using an elastic wave equation estimate multiple parameters representing different physical properties of the subsurface, which increases the null space of the parameter space, leading to a larger domain of ambiguity and increasing the number of models that can equally well explain the data. Third, because elastic parameters have similar radiation patterns, interparameter crosstalk may occur causing updates of one parameter to leak into other, which results in artifacts in the inverted model. In addition, as multiple elastic parameters are updated simultaneously, but independently, the inversion may deliver artifact-contaminated or unphysical models (e.g., negative Poisson ratio) that do not represent plausible lithological units.

To mitigate the intrinsic problems of EFWI and thus produce geological plausible elastic models, many authors propose incorporating penalties or a regularization term based on petrophysical information in the inversion objective function (Asnaashari et al., 2013; Duan and Sava, 2016; Zhang et al., 2018; Rocha and Sava, 2018; Zhang and Alkhalifah, 2019). However, the techniques proposed by these authors present many limitations, which are discussed in Aragao and Sava (2019a,b). Here, we discuss this novel, general, flexible, and automated technique to incorporate petrophysical information into EFWI. We explicitly exploit the petrophysical data as penalties to guide models toward realistic lithology using multiple probability density functions (PDFs) estimated without user-defined parameters, in order to avoid assuming explicit and potentially inaccurate petrophysical relations among the parameters. We build the multiple PDFs by dividing the well log data into different lithological units (*clusters*), by using a classification method, such as K-means clustering (MacQueen, 1967).

Method

We solve the inverse problem by minimizing an objective function $\mathscr{J}$ composed by the data misfit term $\mathscr{J}_D$ and a term that applies model constraints using a petrophysical penalty term, $\mathscr{J}_P$. We computed the modelled data by considering the isotropic elastic wave equation

$$\rho\ddot{\mathbf{u}} - \lambda[\nabla(\nabla\cdot\mathbf{u})] - \mu\left[\nabla\cdot\left(\nabla\mathbf{u}+\nabla\mathbf{u}^T\right)\right] = \mathbf{f}, \tag{1}$$

where $\mathbf{u}(e,\mathbf{x},t)$ is the elastic displacement, $\mathbf{f}(e,\mathbf{x},t)$ is the source function, $\rho(\mathbf{x})$ is the density, e, $\mathbf{x}$ and t are, respectively, the experiment index, space coordinates and time, and $\lambda(\mathbf{x})$ and $\mu(\mathbf{x})$ are the Lamé parameters.

In order to calculate $\mathscr{J}_P$, we classify the petrophysical data, such as well logs, into a number of clusters (lithological units), that we use to build the different PDFs. Each PDF is represented by coordinates $\mathbf{p}$, while the components of the model parameters are represented by the vector $\mathbf{m}(\mathbf{x}) = \{\lambda(\mathbf{x}), \mu(\mathbf{x})\}$. Then, for any given model represented by $\mathbf{m}$, we use the closest PDF to compute a distance to any point of this distribution by

$$d(\mathbf{m},\mathbf{p}) = \|\mathbf{m}-\mathbf{p}\|_2. \tag{2}$$

We also use the probability density $f(\mathbf{p})$ described by each PDF in order to determine the distance $D(\mathbf{m})$

from $\mathbf{m}$ to the entire distribution as

$$\frac{1}{D(\mathbf{m})} = \sum_{\mathbf{p}} \frac{f(\mathbf{p})}{d(\mathbf{m},\mathbf{p})}. \tag{3}$$

Finally, the penalty term $\mathscr{J}_P$ is defined as

$$\mathscr{J}_P = a \sum_{\mathbf{m}} D(\mathbf{m}), \tag{4}$$

where the scalar parameter a determines the strength of the penalty term in the objective function. The gradients of $\mathscr{J}_P$ with respect to the model parameters λ and μ are, respectively,

$$\frac{\partial \mathscr{J}_P}{\partial \lambda} = a D^2(\mathbf{m}) \sum_{\mathbf{p}} \frac{f(\mathbf{p})(\lambda - \lambda_p)}{d^3(\mathbf{m},\mathbf{p})}, \tag{5}$$

and

$$\frac{\partial \mathscr{J}_P}{\partial \mu} = a D^2(\mathbf{m}) \sum_{\mathbf{p}} \frac{f(\mathbf{p})(\mu - \mu_p)}{d^3(\mathbf{m},\mathbf{p})}. \tag{6}$$

For illustration, consider the PDF depicted in Figure 1a representing petrophysical information. Figure 1b shows the distribution of $D(\mathbf{m})$, which is small in the proximity of the given PDF and increases away from the distribution. Figure 1c displays the distribution of the gradient of $D(\mathbf{m})$, which is close to zero in the region where the PDF is high. Thus, once a point $\mathbf{m}$ in the updated model is consistent with the distribution given by the PDF, the data misfit $\mathscr{J}_D$ fully controls the gradient and the action of the petrophysical penalty term ceases.

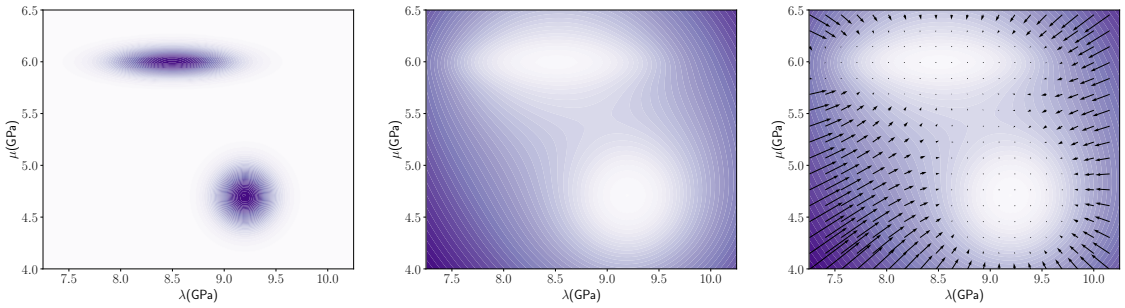

(a) (b) (c)

Figure 1 *(a) Example of a PDF consisting of two Gaussian functions, (b) the distance $D(\mathbf{m})$ and (c) its gradient. Note that high probability models are associated with small values of $D(\mathbf{m})$ and with zero gradients.*

Examples

We illustrate the technique with a portion of the Marmousi 2 model. Figures 2a and 3a show, respectively, the correct λ and μ models. We consider wells located at $x = 0.5$ km, $x = 1.5$ km and $x = 2.5$ km for building the petrophysical penalty $\mathscr{J}_P$. We use K-means clustering in order to divide the petrophysical information into 4 clusters, i.e., to build 4 different PDFs. We simulate a multicomponent survey with a line of receiver at $z = 0.05$ km and 75 evenly spaced sources located at $z = 0.025$ km. Figures 2b and 3b show the initial model parameters.

Figures 2c and 3c show the recovered models using the objective function $\mathscr{J}_D$. Both the recovered λ (Figure 2c) and μ (Figure 3c) models are contaminated with high-wavenumber artifacts in addition to the artifacts due to the inherent interparameter cross-talk of EFWI. Furthermore, the inversion is not able to produce long-wavelength updates which deteriorates the quality of the recovered models, thus resulting in models with poor resolution (Figures 2c and 3c). Additionally, as the elastic parameter μ only depends on the velocity of shear waves when viscoelasticity is not being considered, the inverted μ model (Figure 3c) has a higher resolution, thus more structural detail, than the inverted λ model (Figure 2c).

Figures 2d and 3d show the recovered models using the objective function $\mathscr{J}_D + \mathscr{J}_P$. Note that the inversion is able to deliver long-wavelength updates while mitigating the interparameter crosstalk artifacts that are encountered in the models recovered using an objective function that only exploits the mismatch in seismic data (Figures 2c and 3c). Additionally, the inversion successfully resolves the structural details presented in the true models (Figures 2a and 3a), resulting in high resolution inverted models.

Conclusions

We explicitly incorporate petrophysical information into elastic FWI to seek both high-quality and high-resolution feasible earth models. We include a penalty term in the objective function based on a probabilistic approach that takes into account the occurrence of many lithological units in the subsurface, which impedes the inversion to deliver unphysical models, while reducing the interparameter crosstalk artifacts. In critical applications, as reservoir characterization, feasible models of subsurface elastic properties are needed to deliver an image with the correct position of geological interfaces. In this way, the proposed framework for FWI can become a state-of-art-technique for estimating accurate subsurface models of elastic properties, allowing for correct image interpretation, and for an understanding of detail complex subsurface structures.

References

Aragao, O. and Sava, P. [2019a] Elastic full waveform inversion probabilistic petrophysical model constraints. *SEG International Exposition and 89th Annual Meeting*, Expanded Abstracts, 1425–1429.

Aragao, O. and Sava, P. [2019b] Elastic wavefield tomography using probabilistic petrophysical clustering. *SEG International Exposition and 89th Annual Meeting*, Expanded Abstracts, 1420–1424.

Asnaashari, A., Brossier, R., Garambois, S., Audebert, F., Thore, P. and Virieux, J. [2013] Regularized seismic full waveform inversion with prior model information. *Geophysics*, **78**, R25–R36.

Duan, Y. and Sava, P. [2016] Elastic wavefield tomography with physical model constraints. *Geophysics*, **81**, R447–R456.

MacQueen, J.B. [1967] Some methods for classification and analysis of multivariate observations. In: *5th Berkeley Symposium on Mathematical Statistics and Probability*.

Operto, S., Gholami, Y., Prieux, V., Ribodetti, A., Brossier, R., Metivier, L. and Virieux, J. [2013] A guided tour of multiparameter full-waveform inversion with multicomponent data: from theory to practice. *The Leading Edge*, **32**, 1040–1054.

Plessix, R.E. [2006] A review of the adjoint-state method for computing the gradient of a functional with geophysical applications. *Geophysical Journal International*, **167**, 495–503.

Pratt, R.G. [1990] Inverse theory applied to multi-source cross-hole tomography. *Geophysical Prospecting*, **38**, 311–329.

Rocha, D. and Sava, P. [2018] Elastic reflection waveform inversion with petrophysical model constrains. *SEG International Exposition and 88th Annual Meeting*, Expanded Abstracts, 1203–1207.

Tarantola, A. [1988] Theoretical background for the inversion of seismic waveforms including elasticity and attenuation. *Pure and Applied Geophysics*, **128**(1), 365–399.

Zhang, Z. and Alkhalifah, T. [2019] Regularized elastic full-waveform inversion using deep learning. *Geophysics*, **84**, R741–R751.

Zhang, Z., Alkhalifah, T., Naeini, E.Z. and Sun, B. [2018] Multiparameter elastic full waveform inversion with facies-based constraints. *Geophysical Journal International*, **213**, 2112–2127.

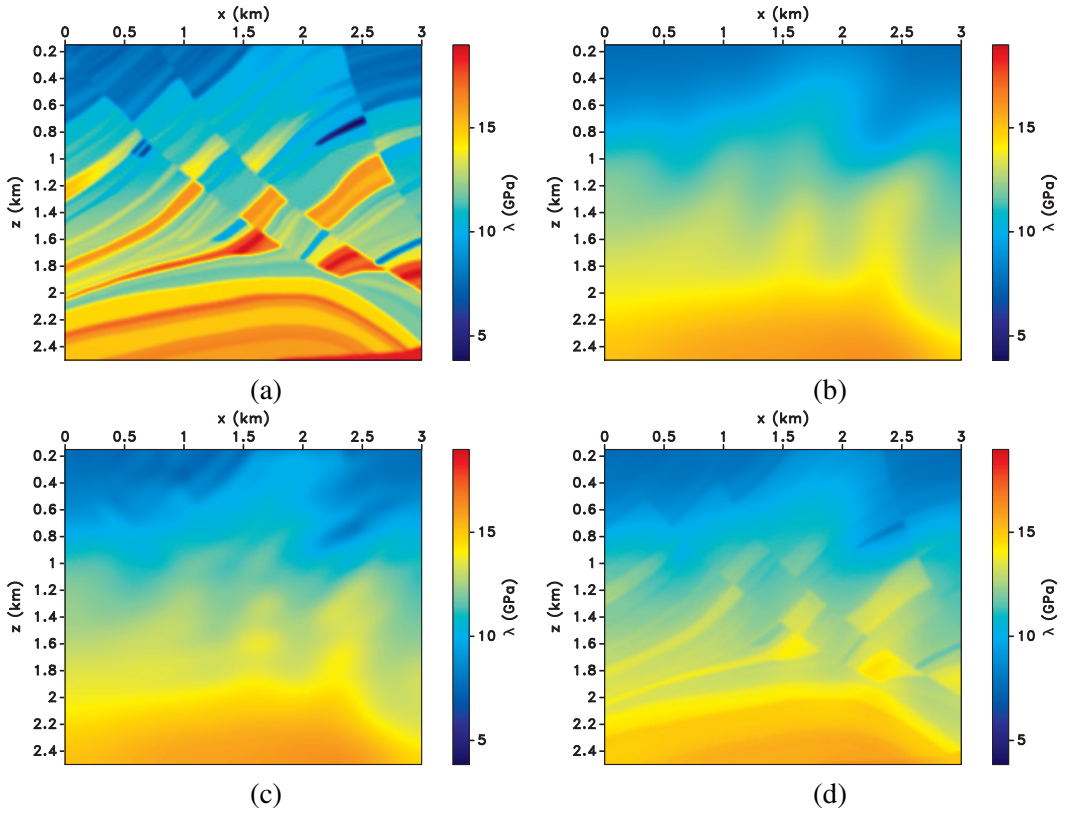

Figure 2 *λ models: (a) true, (b) initial, (c) recovered using the objective function $\mathcal{J}_D$, and (d) recovered using the objective function $\mathcal{J}_D + \mathcal{J}_P$.*

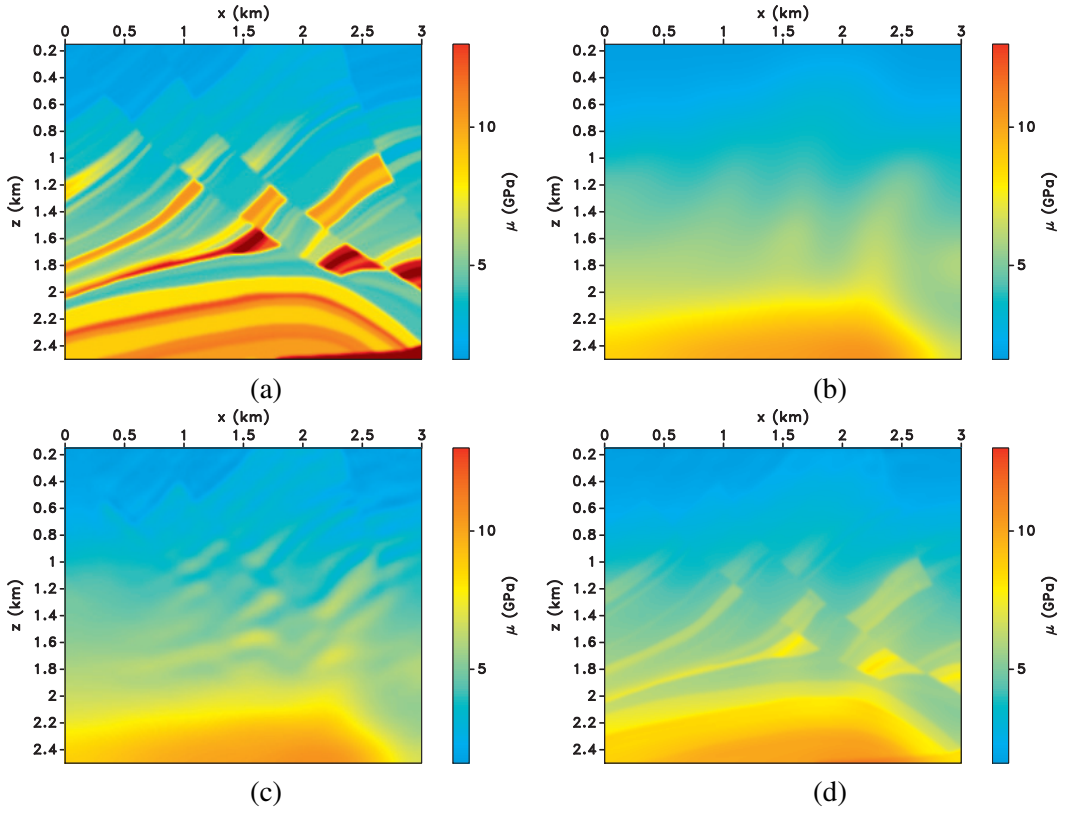

Figure 3 *μ models: (a) true, (b) initial, (c) recovered using the objective function $\mathcal{J}_D$, and (d) recovered using the objective function $\mathcal{J}_D + \mathcal{J}_P$.*